Continuous flow production of size-controllable niosomes using a thermostatic microreactor

Pablo García-Manrique[1,2], Gemma Gutiérrez[2], María Matos[2], Andrea Cristaldi[3], Ali Mosayyebi[3], Dario Carugo[4], Xunli Zhang[3*], María Carmen Blanco-López[1*]

[1]*Department of Physical and Analytical Chemistry, University of Oviedo; Spain*
[2]*Department of Chemical Engineering and Environmental Technology, University of Oviedo; Spain*
[3]*Bioengineering Sciences Group, School of Engineering; Institute for Life Sciences (IfLS), University of Southampton; United Kingdom*
[4]Mechanotronics and Bioengineering Sciences Research Groups, *School of Engineering; Institute for Life Sciences (IfLS), University of Southampton; United Kingdom*

Corresponding authors: *E-mail address*: cblanco@uniovi.es, XL.Zhang@soton.ac.uk

This article contains 8 figures and 6705 words (including the abstract). The supplementary material includes 3 figures and 2 tables.

Abstract

The new roles of vesicular systems in advanced biomedical, analytical and food science applications demand novel preparation processes designed to reach the new standards. Particle size and monodispersity have become essential properties to control. In this work, key parameters, involved in a microfluidic reactor with hydrodynamic flow focusing, were investigated in order to quantify their effects on niosomes morphology. Particular attention was given to temperature, which is both a requirement to handle non-ionic surfactants with phase transition temperature above RT, and a tailoring variable for size and monodispersity control. With this aim, niosomes with two different sorbitan esters and cholesterol as stabilizer were formulated. High resolution and conventional 3D-printing technologies were employed for the fabrication of microfluidic reactor and thermostatic systems, since this additive technology has been essential for microfluidics development in terms of cost-effective and rapid prototyping. A customised device to control temperature and facilitate visualization of the process was developed, which can be easily coupled with commercial inverted microscopes. The results demonstrated the capability of microfluidic production of niosomes within the full range of non-ionic surfactants and membrane stabilizers.

Keywords

Organic colloids, Niosomes, Size control, Hydrodynamic Flow-Focussing, Microreactor, 3D-printing

1. Introduction

A precise control over local environment during production of colloids is essential to minimise perturbations in chemical characteristics that could lead to heterogeneous populations, and then, differences in particle properties. To achieve such homogeneity and uniform properties, a strict control of particle size is necessary [1,2].

Nanovesicles (organic colloids) are particles formed by self-assembled amphiphilic molecules into closed bilayered structures with an inner aqueous core. Depending on the chemical nature of bilayer constituents, these particles are categorised into liposomes (lipids), niosomes (non-ionic surfactants) or polymersomes (block copolymers), as most frequently found in the literature [3,4,5].

Niosomes exhibit unique advantages over the other types of vesicular systems due to their inherent characteristics of non-ionic surfactants [6,7]. These advantages include; (i) better chemical and physical stability of suspensions due to the absence of oxidation-related

degradation, (ii) easy derivatization to introduce different functional groups for stability enhancement or bioconjugation, (iii) wide range of surfactant types available (with single or double acyl chain, with different length or saturation), (iv) high immunological tolerance, and (v) cost effectiveness. Firstly introduced in the cosmetic industry by L'Oreal [8] for dermal bioactive compounds delivery, over the last 15 years their applications have expanded to many fields. Food fortification [9], diagnostic agents [10], analytical chemistry [11], nanomaterial synthesis [12], and drug delivery [13] are just some of examples. For all of these applications, a product with specific characteristics, homogeneity and reproducibility is desired, and in particular, controlled size and monodispersity are essential.

Effort has been made to the production of niosomes by traditional methods with tight control over size and size distribution [14] for some specific applications [15]. For example, in our previous work [16], we have used experimental design to study the influence of variables in the ethanol injection process, in order to improve particle size tunability.

One of the most popular chemical families for niosome production involves sorbitan esters (commercially available as Span®). Span family members differ in terms of acyl chain length and saturation, with a big range of hydrophilic-lipophilic balance values (HLB), where HLB is an important parameter with implications in drug encapsulation efficiency and morphological characteristics of particles. This parameter is also related to the physical state at room temperature (RT), and influences the minimum temperature (together with *gel-to-liquid* transition temperature, or T_c) that is required at the very stage of the particle formation. On the other hand, some of the compounds used in formulations with great loading capacity, low release rate and stability in solution are solid at RT. For these reasons, a higher and controlled temperature level is mandatory for this process.

Microfluidics technology is very promising for precise control over input variables when mixing chemical species [17]. Other advantages include low consumption of chemicals (relevant in formulation optimization), scale-up possibilities for industrial production, on-line coupling to other processes (such as purification steps), and efficient control over temperature if required [18]. Jahn et al. [19] reported for the first time the hydrodynamic flow focussing (HFF) technique (**Figure 1**) for liposomes production. Following that, other researchers have used this method to examine various liposomes formulations and for encapsulating either hydrophobic or hydrophilic molecules [20,21]. Under laminar flow conditions within the HFF configuration, a stream of lipids in organic phase is focussed between two aqueous streams in microchannels, allowing the mixing of chemical species by molecular diffusion. At the two

organic/aqueous interfaces, bilayers can be formed and self-assembled into liposomes once a critical concentration is reached. By controlling the flow, the extension of mixing and hence the size of liposomes, could also be controlled. However, the production of niosomes through microfluidic routes remains less explored, and limited attention has been paid to using HFF technique [22,23,24].

Figure 1

At present, the high temperature required for the preparation of niosomes has not been well taken into account in microfluidics routes. For example, the previous work that firstly explored microfluidics assembly of niosomes faced such temperature related challenge, thus only included Span® 20 and Span® 80 (T_m = 25 °C and -30 °C, respectively) in the study. [22]

Along with the wide application of continuous flow microreactors for organic colloids preparation[18] is the development of microreactor itself, including design and manufacturing of such microdevices, with simpler and more affordable production methods [25]. As a result, some traditional fabrications methods which stem from the photo-electronics field, such as photolithography [26], are being substituted by new processes that require less expensive equipment and can be performed in common labs with no need for clean rooms facilities [27]. Among the techniques explored, additive manufacturing, especially 3D-printing, has emerged as a promising method for microfluidic device manufacturing [28]. The rapid development of 3D-printing technology and the commercialization of desk printers have enabled researchers to explore its utility in microfluidic prototyping and manufacturing [29,30,31], that generally use low cost raw materials and can print objects with desired resolution.

The aim of the present work was to develop a thermostatic microreactor platform for the continuous flow production of niosomes in a size-controllable manner. The microfluidic reactor was designed with a hydrodynamic flow focusing configuration, and fabricated in order to allow visualization of the dynamic process including molecular diffusion, with the aid of an inverted microscope and a digital image acquisition system. 3D-printing technology was used for fabricating the microfluidic device (positive mould) and thermostatic system. The effect of operational parameters was investigated on the final morphological characteristic of niosomes. Niosomes were formulated with non-ionic surfactants with different transition temperatures (T_m) with controlled temperature as a tailoring parameter to tune the size and homogeneity of particles.

2. Materials and methods

2.1 Materials

Sorbitan monostearate or Span® 60 (Sigma-Aldrich), sorbitan monolaureate or Span® 20 (Sigma-Aldrich), cholesterol from lamb wool (Akros Organics), Phosphate Buffer Saline (10 mM, pH 7.4) prepared from tablets according to manufacture instructions (Sigma-Aldrich), Bromoxylenol blue (Sigma-Aldrich), and technical grade solvents such as ethanol absolute, 2-propanol (or isopropyl alcohol, IPA), and acetone (all from J.T. Baker, Avantor, USA) were used in this work. Ultrapure water was used for all experiments. Poly(dimethylsiloxane) monomer Sylgard® 184 or PDMS was purchased from Dow Corning Corporation (Auburn, AL, USA). Other materials used for devices fabrication are specified in the following respective sections.

2.2 Thermostatic system fabrication

Thermostatic chamber was design in Autodesk® Inventor® and 3D-printed with PLA filaments using a special printer for fused deposition modelling (Ultimaker 2+ 3D printer, Ultimaker B.V., The Netherlands). Main chamber and cap of the device were produced separately. A microscope glass slide of 50 x 70 mm (Corning® microscope slides, Sigma-Aldrich, Gillingham, UK) was sealed to the chamber with a 2-phase adhesive glue special for plastic materials, bought in a local store. A transparent piece of plastic was glued to the cap aperture with the same adhesive used with the other piece. Teflon tape was used to enhance the closure of both elements in a removable way. Holes for the inlets and outlet pipes of the microfluidic device were manually prepared with a sharp tool.

The previously described chamber was connected to a temperature-controllable recirculation system (F12-MC, Julabo GmbH, Germany) through the inlet, and a peristaltic pump (MasterFlex®, Cole-Parmer Instruments Company, USA) through the outlet. The plastic pipes were those from the recirculator, and connections to the chamber were made with common plastic adapters (see supplementary material).

External supply of the recirculator was set approximately at a flow rate of 55 % of the total volume, while peristaltic pump revolution rate was adjusted to remove water from the chamber at a rate that allowed a continuous and constant flow through it. Temperature inside the chamber was monitored with a digital temperature probe (Testo 110, Testo SE & Co., Germany). The sensor probe was introduced into the chamber through a hole placed in one side of plastic window of the cap (see **Figure S2**).

2.3 Microfluidic devices manufacturing and channel characterization

Master mould of devices was designed in Solidworks® CAD 2016 software and 3D-printed onto VeroClear™ resin with the HR-3D printer Objet350 Connex™ (Stratasys Ltd., USA). A post-printing process was also needed. First, mould was flushed with (I) IPA, (II) deionized water, (III) acetone, and finally compressed air. Then, it was cured overnight at 60 °C, and on the following day a treatment of the inner surface was carried out with Aquapeel® (to avoid interference of the resin with PDMS curing process). Three individual moulds were printed.

Once the positive mould was ready, a mixture of degassed PDMS curing agent (1:10 w/w) was poured into it, and left overnight in an oven at 40 °C. For degassing the PDMS mixture, a bench centrifuge was used at 3000 rpm for 10 min. It should be noted that pouring into master mould must be done slowly to minimise bubble formation. On the following day, the replica of the mould was carefully peeled off from the mould, and inlets and outlet holes were prepared with a 1.5 mm biopsy punch with plunger (Miltex®, Fischer Scientific, UK).

Oxygen plasma (PVA-TePla 300 plasma cleaner, Wettenberg, Germany) treatment was applied to bond a microscope glass slide (50 x 70 mm; Corning® microscope slides, Sigma-Aldrich, Gillingham, UK) to the PDMS replica to complete the microfluidic channel. Four pieces of thermic resistant plastic (Ø 8 mm and 3 mm height) were glued in each corner at the bottom of the glass slide, to elevate the device allowing a flow of hot water under the channels.

Polytetrafluoroethylene (PFTE, 0.5 mm I.D.) pipes (Cole-Parmer, UK) were inserted into the holes, and the other end was attached to a syringe needle to create a connection for introduction of the fluids from syringe pumps (NE-300, NEW ERA Pump Systems Inc., USA). Luer lock syringes (Becton, Dickinson and Company, UK) of 1, 10 or 20 mL were used depending on the selected Flow Rate Ratio (FRR), i.e. volumetric flow rate of total aqueous phase/ volumetric flow rate of organic phase.

The mixing channel (23 mm long) on the 3D-printed positive mould was characterized in terms of morphology, accuracy and reproducibility by mechanical profilometry (Talysurf-120L, Taylor-Hobson, United Kingdom). Three equidistance measurements were taken (2 mm across the channel, perpendicular to it), and data were processed with OriginPro 18 (OriginLab Corporation, USA) software.

The whole setup (microfluidic device inside the thermostatic chamber with respective inlets and outlets) was placed over the stage of an inverted microscope (IN200TAB series, AmScope, USA) with a digital imaging system to capture images (5M.P USB CCD camera, AmScope, USA)

supported with the software supplied by the camera manufacturer. The entire experimental setup is illustrated in **Figure S2**.

2.4 Niosomes production and morphological characterization

Working solutions of 5 and 20 mM of Span® 60:cholesterol and Span® 20:cholesterol (1:0.5 molar ratio) were prepared by dilution from a 50 mM stock solution. Ethanol absolute was used as organic solvent, since it is miscible in aqueous buffer (PBS, 10 mM pH 7.4). Aqueous and organic phases were pumped into microfluidic device once appropriate temperature was reached. Three different total flow rates (Q_T) were studied (50, 100 and 200 µL/min), and aqueous:organic flow rates were adjusted to five different flow rates ratios (FRR) (5, 15, 25, 35 and 50). Span® 20:cholesterol formulation was injected at 30, 40, 50 and 60 °C; while Span®60: cholesterol was only injected at 50 °C. All the combination of membrane components concentration, Q_T, FRR, and temperature was conducted by duplicate.

A total volume of 2.5 mL was collected from the outlet of the device for each experimental condition in a glass vial. Size (z-average or peak value, depending on the number of peaks in the size distribution) and homogeneity (PDI) of particles were measured by Dynamic Light Scattering (DLS) in a Zetasizer NANO-ZS equipment (Malvern Instruments Ltd, Malvern, UK). Samples were measured undiluted by triplicate, with the 173° backscatter detector in disposable low volume cuvettes (Malvern Instruments Ltd, Malvern, UK).

2.5 Mixing efficiency visualization

Solvent and no-solvent diffusion by hydrodynamic flow focusing was monitored by an adaption of a previous published methodology [32]. Briefly, a change in colour of a pH indicator dye (bromoxylenol blue) was used, since this dye exhibits a strong yellowish colour at pH below 6.0 and blue at pH above 7.6. A saturated solution of dye in absolute ethanol acidified with acetic acid was focused by PBS adjusted to pH 10.0 with 2M NaOH solution. Once focused, a change in colour of the stream from yellow blue indicated a molar fraction of aqueous phase close to one, and then, completes mixing by diffusion.

3. Results and discussion

With the microreactor platform developed, systematic characterisation and operation were conducted in terms of 3D printing outcomes and nanoproduction, as detailed below. (The performance and optimization of the thermostatic system are described in the supplementary material, **figure S1**.)

3.1. High resolution 3D-printing of master moulds for microfluidic devices fabrication

As a key element of the device, mixing channel morphology was characterized by mechanical profilometry onto 3D-printed positive moulds. A considerable difference in nominal dimensions between Computer Aided Design (CAD) and printed object was observed (**Table S1**). With an original squared cross sectional geometry of 100 µm width and 100 µm height, printed features onto VeroClear® resin showed a curved morphology five times wider and approximately half of the height. At the same time, variations in width and height of the mixing channel were found between the three 3D-printed positive moulds (see **Table S1**) even following the same fabrication procedure. However, these dimensions were reasonably constant along the mixing channel length, especially for channel height.

A possible explanation for these variations in channel dimensions could be related to printer operational parameters. Objet350 Connex3 printer used Polyjet™ inkjet-head patented technology for a layer-by-layer process based on Stereolithography [33]. The jetting head dispensed a proper amount of a photopolymer resin onto a build tray and instantly cured them with UV light. The process took place in XY-axes to create a 2D sheet (down to 16 microns thickness), and by lowering the build tray, another layer was created over the previous one. The cycle was repeated until the whole design was completed. With a resolution of 600 x 600 x 1600 dpi (X-Y-Z-axes respectively) and an accuracy of 20-85 microns for features below 50 mm (up to 200 microns for full model size), the final features depended on geometry (proximity between elements), build parameters (exposure time, printing speed) and model orientation [29]. Comina et al. [29] reported the successful printing of positive moulds for microfluidics devices with elements from 50 µm to 2 mm, however, some artefacts were described between close elements with 50 µm in dimension differences, though working with optimized parameters. Unfortunately, no details about cross section geometry were given for these channels. Some other authors [34] have reported differences between CAD and printed designs with efforts in resin formulation optimization.

In our recent work [31], we found that 3D printed channels with the Objet350 Connex3 printer were smoother than channels printed with a conventional desk 3D printer (Ultimaker 2+). However, for the same dimensions and aspect ratio, accuracy in cross sectional shape was lower for the HR-3D printer even at large dimensions (1 mm squared channels). It suggested that further studies are needed to understand this effect with the scale and for different materials in order to inform printing parameters optimization in terms of element dimensions, geometry, and printing materials. Apart from the difference between CAD and 3D-PMs, the

cross sectional area of Mould 3 was similar to that previously used by Lo et al. [22], on which the selected operational parameters of the present work were based.

3.2. Production of nanoparticles with temperature control for formulations with high T_m non-ionic surfactants

The use of non-ionic surfactants for the formulation of organic colloids, especially for NVs preparation, exhibits numerous advantages [4,6]. However, a strict control of the temperature is necessary if Span®60 (T_m = 45 °C), one of the most commonly used surfactant in niosome formulation) is involved. **Figure 2** shows its precipitation at RT in microchannels once reaching the focusing region, highlighting the significance of temperature effect.

In Figure 2 surfactant precipitation was observed at the focussing region and persists along the channel length when Span® 60 is used at 25 °C. However, at 50 °C a complete mix of both phases were produced without the presence of any surfactant precipitation. Moreover, the production of niosomes at this temperature conditions were observed using Transmission Electron Microspcopy (TEM) and negative staining protocol.

Figure 2

This technique has been less explored than traditional bulk preparation routes [18], and with important advantages such as better control over particle preparation and the subsequent final characteristics (size and monodispersity, i.e.). This is important for biomedical [1], food [35] and analytical chemistry [2] applications. In this regard, the influence of operational conditions over particles physical properties was tested by analysing the results of 3 total flow rates (Q_T), two different concentrations of bilayer components, for 5 different FRR. Particle size (nm) and size distribution (PDI) were measured by DLS as output variables. All the combinations were conducted at 50 °C, a temperature over surfactant T_m.

In general terms, smaller particles were produced as the FRR increased (F**igure 3A and 3B**) for both concentrations (5 and 20 mM), and for all the Q_T levels. At a concentration of 5 mM (Figure 3A), the particle size decreased from 278, 298 and 358 nm (when FRR = 5) to 155, 129 and 143 nm (when FRR = 50), where Q_T = 50, 100 and 200 µL/min, respectively. At a concentration of 20 mM (Figure 3B), similarly, the particle size reduced from 342, 361 and 386 nm (when FRR = 5) to 164, 147 and 151 nm (when FRR = 50) at the three Q_T levels of 50, 100 and 200 µL/min, respectively. Size reduction was rapidly reached with an increment in FRR from 5 to 15, and this reduction became less pronounced from FRR 15 to 50. It is important to

take into account that when FRR increased the total amount of bilayer components decreased, not only producing vesicle with smaller size, since particle concentration was also reduced.

No significant effect of different Q_T was observed, while only some differences were noticed in some particular combinations of parameters at low surfactant concentration (5 mM), as seen in Figure 3A. These observations were in accordance with previous studies [22] carried out with identical chip configuration for the production of niosomes formulated with other sorbitan esters (Span®20 and 80), and also for the production of liposomes [19,20,36,37]. At lower Q_T, also the linear velocity was lower (hence larger residence time) what can counteract the effect of the bilayer components concentration.

Figure 3

The increase in FRR, and the subsequent decrease in initial focused width (W_f), reduced the time needed for a complete mixing between solvent and no-solvent (t_{mix},), thus the critical concentration to induce molecules self-assembly was reached faster. This led to smaller vesicles since the total amount of bilayer components was reduced [38]. On the other hand, the reduction of solvent introduced in the mixing channel also decreased the possibility of particle fusion into bigger unities by Ostwald-ripening phenomena [20,39]. A reduced t_{mix} also led to complete mixing in limited length channels. In other cases, no diffused solvent containing amphiphilic molecules self-assembled out of the channel under entirely different conditions (outlet pipes, with no laminar flow characteristics).

Regarding size distribution of particles (F**igure 3C and 3D**), PDI value reduced as FRR increased from 5 to 15, (for 5 mM: from 278, 298 and 358 nm at FRR = 5 to 155, 129 and 143 nm at FRR = 50; for 20 Mm: from 342, 361 and 386 nm at FRR = 5 to 164, 147 and 151 nm FRR = 50; for both concentration values are indicated for Q_T = 50, 100 and 200 µL/min respectively). and remained without significant changes at higher FRR for both concentrations. Some authors [19,20,32] reported a significantly increase in PDI with the increment of FRR for an identical chip configuration, but for liposomes production instead. However, our observation was in line with that of Bottaro et al. [32] in a "Y"-shaped device, while Joshi et al. [21] described also a reduction in PDI as FRR increase during liposome formation. No significant differences on PDI were observed for all Q_T levels applied.

The use of microreactors with different channel configurations, and the use of static mixing enhancers [40], could be the reason of different results among published works. Some of them have highlighted the influence of channel dimensions and configurations over mixing efficiency and particle properties [19,22,36]. The preparation of solvent mixture containing bilayer

309 precursors can also influence the extension and homogeneity of solubilisation, and in
310 consequence, nanoprecipitation process. In the present work, ethanol was used as solvent for
311 microfluidic-based preparation of niosomes for the first time, and this limited the possibility
312 for comparison with other studies.

313 We have noticed that at high FRRs some transitory perturbations of the focused fluid were
314 recorded, especially at 50 µL/min. The focused stream exhibited a "beating pulse" like effect
315 that was likely produced by the syringe pump due to its own pumping mechanism. These
316 pulses created really short increments in the width of the focused fluid that introduced
317 alteration in solvent exchange kinetics and the subsequent changes in the local concentration
318 of bilayer precursors and solvent concentration.

319 Surprisingly, lower PDI values were obtained at 20 mM for all FRRs at the three different Q_T.
320 Indeed, these differences were higher at 50 µL/min. At low concentration, those mentioned
321 instabilities can induce more pronounced local changes in bilayer precursor's abundances, with
322 the corresponding effect in particle monodispersity. To gain insights into these observations
323 further studies are needed.

324 On the other hand, larger particles were obtained when a higher concentrated ethanolic
325 solution of bilayer components was used (20 mM *vs.* 5 mM). This was observed at all Q_T and
326 FRR levels (see supplementary material, Figure S4). The same observation was also reported by
327 other authors when producing liposome using microchannels [37], and in agreement with the
328 mechanism of vesicle formation under microfluidic flow dynamic mixing.

329 The efficiency of mixing under the assayed working conditions was studied following a
330 published methodology [32]. With this method, mixing efficiency was measured through the
331 change in colour of a pH indicator dye (bromoxylenol blue), that changed from yellow (acidic
332 ethanolic solution containing bilayer precursors) to blue (basic aqueous phase, PBS pH= 10). A
333 shift in focused fluid colour from yellow to blue indicated that molar fraction of water into the
334 stream was close to 1 and the subsequent molar fraction of EtOH became close to 0,
335 evidencing a complete mixing by solvent and aqueous effluents. This change in colour was
336 easily detected in the inverted microscope, and recorded with the digital camera. As an
337 example, results for Q_T = 100 µl/min at several FRRs are shown in **Figure 4**.

338 **Figure 4**

339 Complete mixing was only reached at high values of FRR (35 and 50) for Q_T = 50 µl/min and
340 Q_T = 100 µl/min, and only at the high FRR (50) for Q_T = 200 µl/min. As Q_T increased, residence

time of the fluid inside mixing channel reduced (from 0.5 s at 50 µl/min to 0.13 s at 200 µl/min), preventing to stay the necessary time to reach complete mixing. Only at high FRR value, t_{mix} was short enough to be compatible with low values of residence time for our channel dimension (t_{mix} = 17 ms and 8 ms for FRR = 35 and 50, respectively, predicted according to a theoretical model (**Equation 1,** [41]). In this model W_f represents the width of focused stream, where w is the channel width and D is solvent diffusion coefficient.

$$t_{mix} \sim \frac{W_f^2}{4D} \approx \frac{w^2}{9D\,(1+FRR)} \qquad \textbf{(Eq. 1)}$$

As seen in Figure 4, W_f decreased as FRR increased, and a dependence of W_f with Q_T was observed at lower FRR values (**Figure 5A**). It was also observed that a lower Q_T generated wider focused streams probably due to the lower pressure exercised by the lateral aqueous flows to the middle solvent flow, but these differences became less pronounced at higher FRRs. A similar trend was observed by Bottaro et al. [32] in an identic channels configuration, but contrary to Jahn et al. [19] who reported a non-variation in W_f with modifications in Q_T.

Figure 5

Moreover, an intense inverse correlation (potential) between FRR and W_f was observed at all the Q_T levels (**Table S2**). However, a strong negative correlation (linear) between particle size and W_f was observed at the two different concentrations studied. These correlations reflect that particle size is governed by focusing parameters. It is clear that niosomes size can be tuned with the selection of the appropriate FRR and Q_T values, which are key parameters for W_f and residence time.

3.3 Production of niosomes at different temperatures to study potential tailoring effect over particle morphology

In this part of work Q_T of 100 µL/min and 5 mM of components concentration were selected, since these have been the best operating conditions in terms of smaller particles with narrower size distributions.

The effect of temperature was examined in a rage of 30 °C and 60 °C as another operating parameter on size-tuned niosomes formation through flow-focused based microfluidics. For this purpose, a non-ionic surfactant with low T_m was needed that allowed to test a wide range of working temperatures. Sorbitan monolaureate or Span® 20 (T_m = 25 °C and HLB 8.6) was selected, another common surfactant used for niosomal formulations [42], and

surfactant:cholesterol molar ratio was kept in 1:0.5 as for Span® 60 in order to allow formulations comparisons.

Figure 6

Figure 6 depicts the results of particle size at the same FRRs previously used for Span® 60 niosomes at different working temperatures: 30, 40, 50 and 60 °C. At 30 °C, a reduction in particle size from FRR=5 to FRR=15 was observed. As FRR increased size became also larger (even higher that those particles produced at FRR = 5). This phenomenon could be related to the observation of cholesterol precipitates inside the mixing channel that were formed immediately after focusing region. The low solubility of cholesterol in water at nearly room temperature induced its precipitation as crystals. Those precipitates modified the flow properties and introduced turbulences that induced micro domains in the fluid with different concentrations of bilayer components, and particles with different morphologies. Also the depletion of cholesterol could generate different particles than those produced in their presence. These perturbations were magnified at higher FRR, since as seen in **Figure 6B** the width of focused fluid became smaller with the increment of FRR, and this stream was relatively smaller than the formed crystals (around 100 µm structures).

For the rest of temperatures, a similar behaviour as for Span® 60 niosomes was observed. Particles size became smaller with an inverse correlation with FRR. At higher temperatures, focused ethanol stream was wider, and these differences were reduced with the increment in FRR. Only slight differences in particle size could be detected (**Figure 6A)**.

Regarding temperature effect some authors reported an increase in particle size as temperature increased [24] which were attributed to the bilayer expansion at higher temperature [43]. In our case, such increase in particle size was not observed. It is know that collapse pressure and surface compressional moduli decrease with temperature for all surfactants, and this implies that Span monolayers are more expanded with increments in temperature. However, as temperature increases planar bilayer precursors are less rigid, which could be easily bended to closed structures, and this effect could lead then to smaller particles [38].

Regarding size distribution and temperature, it was observed that the increment of temperature yielded more monodisperse particles, especially at 50 °C. Complete mixing can be reached at FRR = 35 and FRR = 50 at any temperature. Only at 50 and 60 °C PDI values remained nearly constant (after a first reduction from FRR=5 to 15) with the increment in FRR.

3.4 Effect of surfactant acyl chain length over particles size and monodispersity

Another interesting finding resulted from the comparison between niosomes formulated with different non-ionic surfactants under identical preparation conditions. In this work niosomes with sorbitan esters with different saturated acyl chain lengths (C12 and C18 for Span® 20 and 60 respectively) were prepared. As seen in **Figure 7**, shorter chains generally yielded larger niosomes. That was contrary to what would be expected; it is generally understood that shorter chains increase the curvature radius of the bilayer, according to the critical packing parameter (cpp) of the molecules [6], allowing smaller particles. However, if was taken into account the higher hydrophilic character of Span® 20 compared to Span® 60 (higher HLB value) the higher hydrophilicity could enhance water soak into the inner core of the vesicle, resulting in larger vesicles size. Similar results were reported by Gutierrez et al. [44] when niosomes were prepared by mechanical agitation. Regarding niosome size distributions, no differences between both types of surfactants were observed.

Figure 7

Conclusions

Novel prototyping and additive manufacturing techniques with such as (HR)3D-printing have been applied for the fabrication of a microfluidic continuous flow reactor for hydrodynamic flow focusing at controlled temperature compatible with commercial inverted microscopes. Despite some alteration in cross sectional dimensions and morphology accuracy with respect to the original CAD design, high resolution 3D-printed positive moulds allow us to create functional microreactors for organic colloid production under different working conditions, and to study their effect on aqueous/solvent mixing efficiency through molecular diffusion, and its relationship with particles morphology.

This work shows that temperature is an essential parameter that must be taken into consideration when formulating niosomes with surfactants with T_m over RT. Also it can be used to modify the properties of particles (size and dispersity) produced with non-ionic surfactants with T_m above RT.

We have found that flow focussing at controlled temperature follows the same patterns as for RT, with the ratio between aqueous and solvent streams being the main parameter to control focused stream width and hence, mixing efficiency and kinetics. However, total flow rate only has insignificant effect when FRRs are set to low values, whilst it can influence residence time, and subsequently, mixing efficiency. In general terms, an increase in FRR yields

a focused stream being narrower, and then, smaller particles due to the reduction in residual solvent and the introduction of less amount of bilayer components. This reduction allows complete mixing, even at high total flow rate, resulting in the size distribution of generated particles being more homogeneous. The counterpart is that production yield is reduced, since particles are generated in a less concentrated suspension. Another variable found to be relevant is the component concentration in ethanol feeding solution, with a direct effect on particle size and monodispersity. A more concentrated solution induces an increment in particle size at any total flow rate, but surprisingly, better size distribution. Complementary, we have checked the influence of acyl chain length over particles morphology, and the versatility that introduces this parameter into the properties and functionalities of this type of biomaterial.

The effect of ethanol stratification due to differences in density was not taken into account, which need further investigation in for future work, in particular in its relationship with focusing temperature.

The findings in this works provide valuable information about microfluidics-based production of niosomes at different operational conditions, and are expected to support the expansion of this technique for the preparation of a wider range of organic colloids with important characteristics for related industries with growing interest in different application fields.

Disclosure

The authors declare no conflicts of interest in this work.

Acknowledgements

This work was supported by the Ministerio de Economía y Competitividad (MINECO, Spain), under the Grant CTQ2013-47396-R and MAT2017-84959-C2-1-R. This study was also financed by the Consejería de Economía y Empleo del Principado de Asturias (Plan de Ciencia, Tecnología e Innovación 2013-2017), under the Grant GRUPIN14-022 and IDI/2018/000185. Support from the European Regional Development Fund (ERDF) is gratefully acknowledged. Pablo García-Manrique is especially grateful to C*ampus de Excelencia de la Universidad de Oviedo* and *Banco Santander* for his mobility fellowship for the stay at University of Southampton.

References

[1] Albanese A., Tang P.S., and Chan W.C., The effect of nanoparticle size, shape, and surface chemistry on biological systems, 2012, Annual Review of Biomedical Engineering, 14, 1-16

[2] Kelly K.L., Coronado E. Zhao L.L., and Schatz G., The optical properties of metal nanoparticles: the influence of size, shape, and dielectric environment, 2003, J. Phys. Chem. B, 107(3), 668-677

[3] Tarun G. and Amit K.G., Liposomes: targeted and controlled delivery system, 2014, Durg Delivery Letters, 4(1), 62-71

[4] Abdelkader H., Alani A.W.G. and Alany R.G., Recent advances in non-ionic surfactant vesicles (niosomes): self-assembly, fabrication, characterization, drug delivery applications and limitations, 2013, Drug Deliv., 21(2), 87-100

[5] Lee J.S. and Feijen J., Polymersomes for drug delivery: design, formation and characterization, 2012 , Journal of Controlled Release, 161(2), 473-483

[6] Marianecci C., Di Marzio L., Rinaldi F., Celia C., Paolino D., Alhaique F., Esposito S., Carafa M., Niosomes from 80s to present: The state of the art, Adv. Colloid Interface Sci., 2014, 205, 187−206.

[7] De S. and Prasad M.R., Self-assembled cell-mimicking vesicles composed of amphiphilic molecules: structure and applications, Volume 1, Encyclopedia of biocolloids and Biointerface Science, First Edition, Hiroyuki Ohshima (Ed.), 2016, John Wiley & Sons

[8] Handjani-Vila R., Ribier A., Rondot B.A., and Vanlerberghie G., Dispersions of lamellar phases of non-ionic lipids in cosmetic products, Int. J. Cosmet. Sci., 1979, 1(5), 303-314

[9] Gutiérrez G., Matos M., Barrero P., Pando D., Iglesias O., and Pazos C. Iron-entrapped niosomes and their potential application for yogurt fortification, 2016, Food Science and Technology,74, 550-556

[10] Demir B., Baris B.F., Pinar G.Z., Unak P., and Timur S., Theranostic niosomes as a promising tool for combined therapy and diagnosis: “all-in-one” approach, 2018, Appl. Nano Mater., 1(6), 2827-2835

[11] García-Manrique P., Lozano-Andrés E., Estupiñán-Sánchez O.R., Gutiérrez G., Matos M., Pazos C., Yañez-Mo M., and Blanco-López C., Biomimetic small extracelular vesicles, 3rd GEIVEX Simposium, San Sebastian, Spain, 29-30 September 2016. Poster communication.

[12] De S., Kundu R., and Biswas A., Synthesis of gold nanoparticles in niosomes, J. Colloid. Interface Sci., 2012, 386, 9-15

[13] Bartelds R., Hadi N.M., Pols T., Stuart M.C.A., Pardakhty A., Asadikaram G., and Poolman B., Niosomes, an alternative for liposomal delivery, PLoS ONE, 2018, 13(4), e0194179

[14] Justo O.R. and Moraes Â.M., Analysis of process parameters on the characteristics of liposomes prepared by ethanol injection with a view to process scale-up: Effect of temperature and batch volume. Chem. Eng. Res. Des. 2011, 89, 785−792.

[15] Danaei M., Dehghankhold M., Ataei S., Davarani Hasanzadeh F., Javanmard R., Dokhani A., Khorasani S., and Mozafari M.R., Impact of particle size and polydispersity index on the clinical applications of lipidic nanocarrier systems, 2018, Pharmaceutics, 57(10),1-17

[16] García-Manrique P., Matos M., Gutierrez G., Estupiñán O.R., Blanco-López M.C., Pazos C., Using factorial experimental design to prepare size-tuned nanovesicles, 2016, Industrial & Engineering Chemistry Research, 55(34), 9164-9175

[17] van Swaay D. and deMello A., Microfluidic methods for forming liposomes, Lab Chip, 2013, 13, 752-767

[18] Capretto L., Carugo D., Mazzitelli S., Nastruzzi C., and Zhang X., Microfluidic and lab-on-a-chip preparation routes for organic nanoparticles and vesicular systems for nanomedicine applications, Advanced Drug Delivery Reviews, 2013, 65, 1496-1532

[19] Jahn A., Vreeland W.N., DeVoe D.L., Locascio L.E., and Michael G., Microfluidic directed formation of liposomes of controlled size, Langmuir, 2007, 23(11), 6289-6293

[20] Kastner E., Verma V., Lowry D., and Perrie Y., Microfluidic-controlled manufacture of liposomes for the solubilisation of a poorly water soluble drug, Int. J. Pharm., 2015, 485, 122-130

[21] Joshi S., Hussain M.T., Carla B.R., Anderluzzi G., Kastner E., Salmaso S., Kirby D.J., and Perrie Y., Microfluidics based manufacture of liposomes simultaneously entrapping hydrophilic and lipophilic drugs, International Journal of Pharmaceutics, 2016, 514, 160-168

[22] Lo C.T., Jahn A., Locascio L.E., and Vreeland W.N., Controlled self-assembly of monodisperse niosomes by microfluidic hydrodynamic focusing, 2010, Langmuir, 26(11), 8559-8566

[23] Obeid M.A., Khadra I., Mullen A.B., Tate R.J., and Ferro V.A., The effects of hydration media on the characteristic of non-ionic surfactant vesicles (NISV) prepared by microfluidics, Int. J. Pharm, 2017, 56, 52-60

[24] García-Salinas S., Himawan E., Gracia M., Arruebo M., and Sebastian V., Rapid on-Chip assembly of niosomes: batch versus continuous flow reactors, Appl. Mater. Interfaces, 2018, 10, 19197-19207

[25] Gross B.C., Erkal J.L., Lockwood S.Y., Chen C., and Spence D.M., Evaluation of 3D printing and its potential impact on biotechnology and the chemical sciences, Analytical Chemistry, 2014, 86, 3240-3253

[26] Dong J., Liu J., Kang G., Xie J., and Wang Y., Pushing the resolution of photolithography down to 15 nm by surface plasmon interference, 2014, Sci Rep, 4, 5618

[27] Carugo D., Lee J.Y., Pora A., Browning R.J., Capretto Lorenzo, Nastruzzi C. and Stride E., Facile and cost effective production of microscale PDMS architecture using a combined micromilling-replica moulding (µMI-REM) technique, 2016, 18, 1-10

[28] Au A.K., Huynh W., Horowitz L.F., and Folch A., 3D-Prinded microfluidics, 2016, Angew. Chem. Int. Ed., 55, 3862-3881

[29] Comina G., Suska A. and Filippini D., PDMS lab-on-a-chip fabrication using 3D printed templates, Lab Chip, 2014, 14, 424-430

[30] Hwang Y., Paydar O.H., and Candler R.N., 3D Printed molds for non-planar PDMS microfluidic channels, 2015, Sensors and Actuators A, 226, 137-142

[31] Cristaldi D.A., Yanar F., Mosayyebi A., García-Manrique P., Stulz E., Carugo D., and Zhang X., Easy-to-perform and cost-effective fabrication of continuous-flow reactors for their application for nanomaterials synthesis, N Biotechnol, 2018, 47, 1-7

[32] Bottaro E., Mosayyebi A., Carugo D., and Nastruzzi C., Analysis of the diffusion process by pH indicator in microfluidic chips for liposomes production, Micromachines, 2017, 8, 209

[33] 3D Printing and additive manufacturing-Fifth Edition, Principles and Applications, 2017, Chee Kai Chua andKah Fai Leong (editors), World Scientific Publishing Co. Pte. Ltd. Singapore.

[34] Gaal G., Mendesa M., de Almeideb T.P., Piazzettad M.H.O., Gobbi Â.L., Riul Jr A., and Rodrigues V., Simplified fabrication of integrated microfluidic devices using fused deposition modeling 3D printing, Sens. Actuators B Chem., 2017, 242, 35-40

[35] Ezhilarasi P.N., Karthik P., Chhanwal N., and Anandharamakrishnan C., Nanoencapsulation techniques for food bioactive components: a review, Food Bioprocess Technol., 2013, 6, 628–647

[36] Carugo D., Bottaro E., Owen J., Stride E., and Nastruzzi C., Liposome production by microfluidics: potential and limiting factors, Sci Reports, 2016, 19, 6:25876

[37] Hood R.R. and DeVoe D.L., High-throughput continuous flow production of nanoscale liposomes by microfluidic vertical flow focusing, Small, 2015, 11, 5790-5799

[38] Antonietti M. and Förster S., Vesicles and Liposomes: a self-assembly principle beyond lipids, 2003, Adv. Mater., 15, 1323-1333

[39] Zhigaltsev I.V., Belliveau N., Hafez I., Leung A.K.K., Huft J., Hansen C., and Cullis P.R., Bottom-Up design and synthesis of limit size lipid nanoparticle systems with aqueous and triglyceride cores using millisecond microfluidic mixing, Langmuir, 2012, 28, 3633-3640

[40] Kastner E., Kaur R., Lowry D., Moghaddam B., Wilkinson A., and Perrie Y., High-throughput manufacturing of size-tuned liposomes by a new microfluidics method using enhanced statistical tools for characterization, 2015, Int. J. Pharm., 477, 361-368

[41] Karnik R., Gu F., Basto P., Cannizzaro C., Dean L., Kyei-Manu, Langer R., and Farokhzad O.C., Microfluidic platform for controlled synthesis of polymeric nanoparticles, Nano Lett., 20018, 8(9), 2906-2912

[42] Manosroi A., Wongtrakul P., Mnosroim J., Sakai H., Sugawara F., Yuasa M., and Abe M., Characterization of vesicles prepared with various non-ionic surfactants mixed with cholesterol, Colloids and Surfaces B: Biointerfaces, 2003, 30, 129-138

[43] Peltonen L., Hirvonen J., and Yliruusi J., The effect of temperature on sorbitan surfactant monolayers, Journal of Colloid and interface Sciences, 2001, 239, 134-138

[44] Gutiérrez G., Benito J.M., Pazos C., and Coca J., Evaporation of aqueous dispersed systems and concentrated emulsions formulated with non-ionic surfactants, International Journal of head and mass transfer, 2014b, 69, 117-128

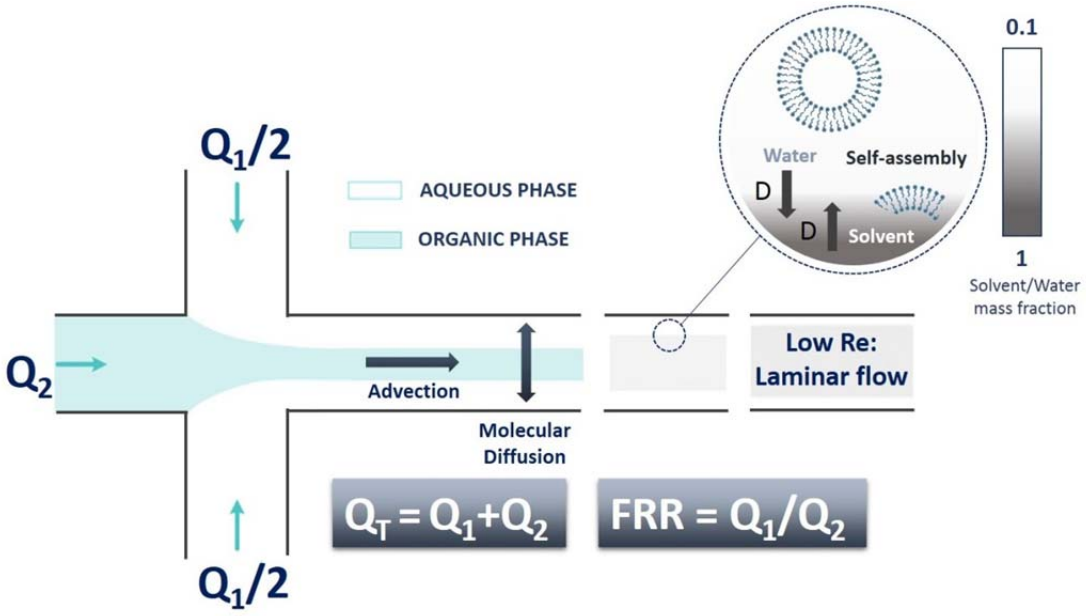
$Q_1/2$
AQUEOUS PHASE
ORGANIC PHASE
Q_2
Advection
Molecular Diffusion
$Q_1/2$
$Q_T = Q_1+Q_2$
FRR = Q_1/Q_2
Low Re: Laminar flow
Water
Self-assembly
D
D
Solvent
0.1
1
Solvent/Water mass fraction

Figure 1.

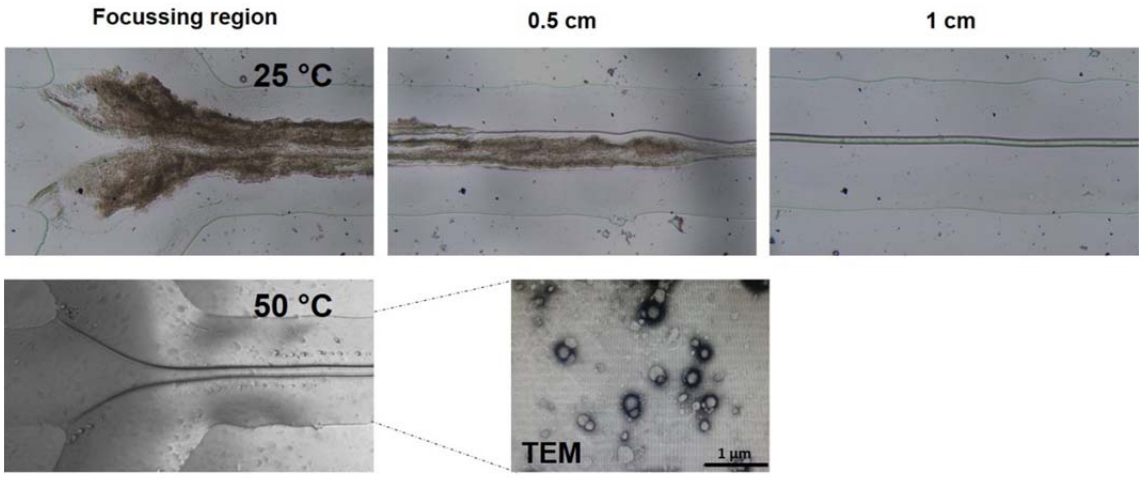

Figure 2.

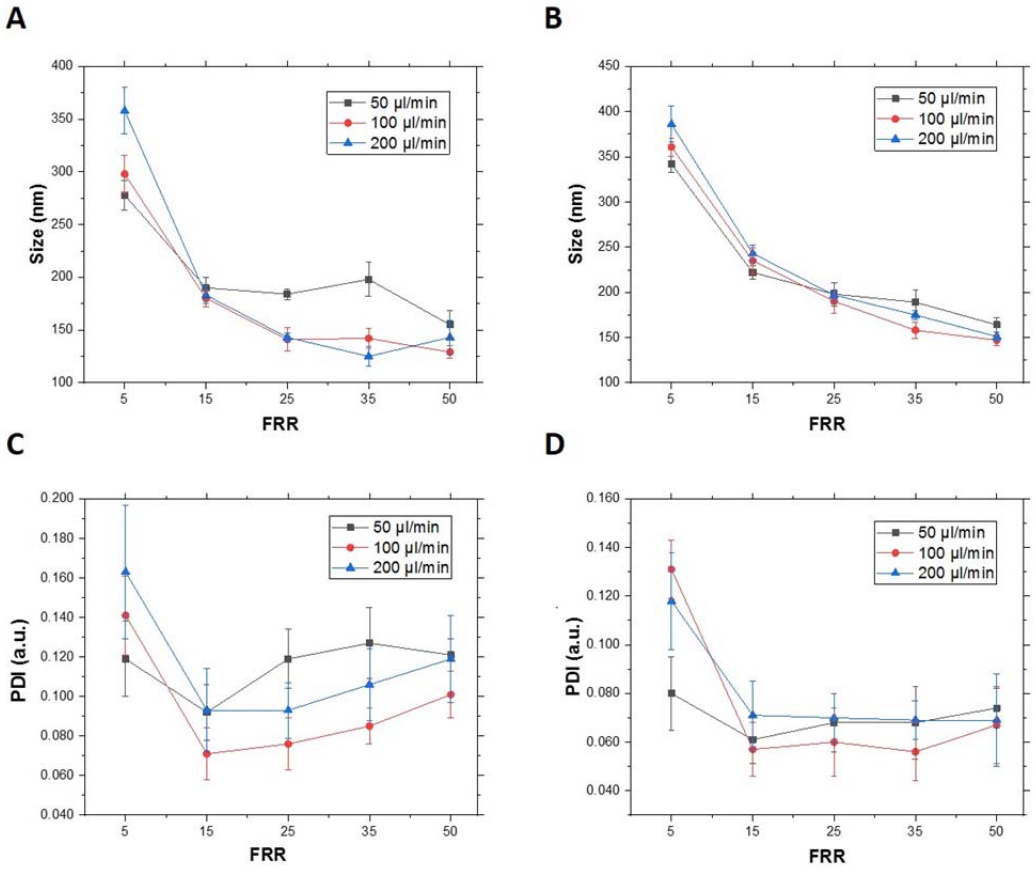

Figure 3.

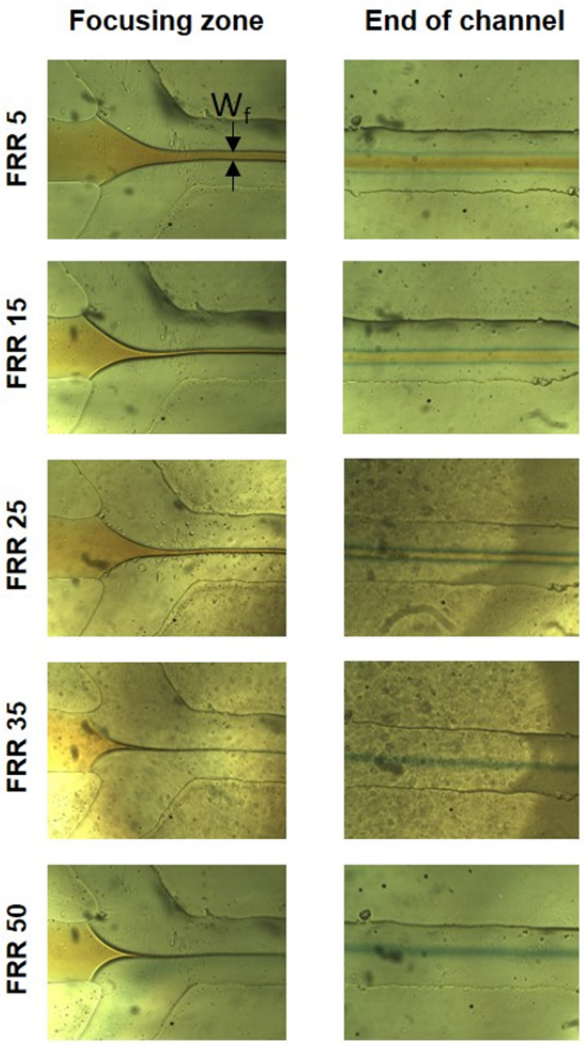
Focusing zone
End of channel
FRR 5
FRR 15
FRR 25
FRR 35
FRR 50
W_f

Figure 4.

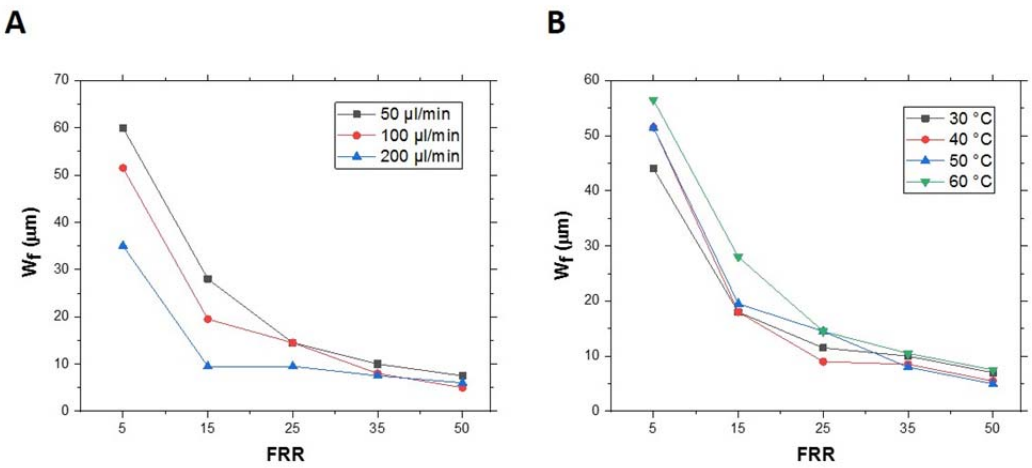

Figure 5.

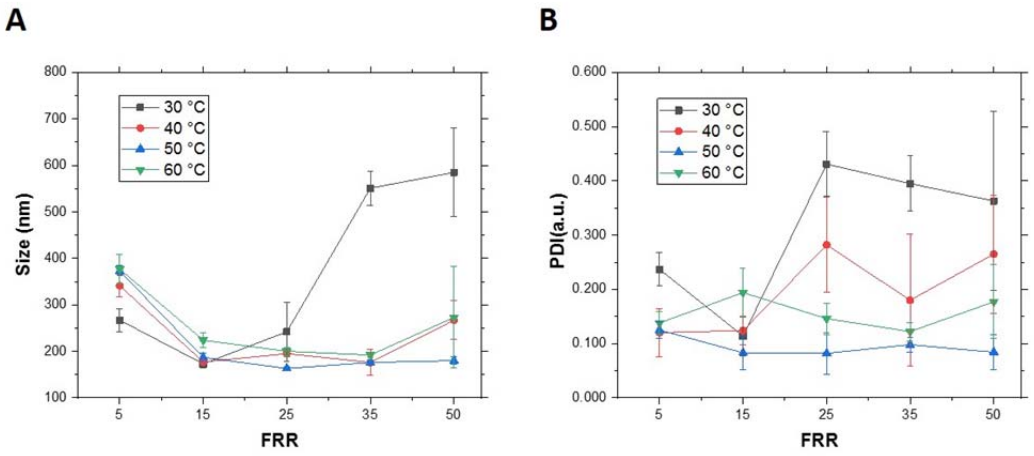

Figure 6.

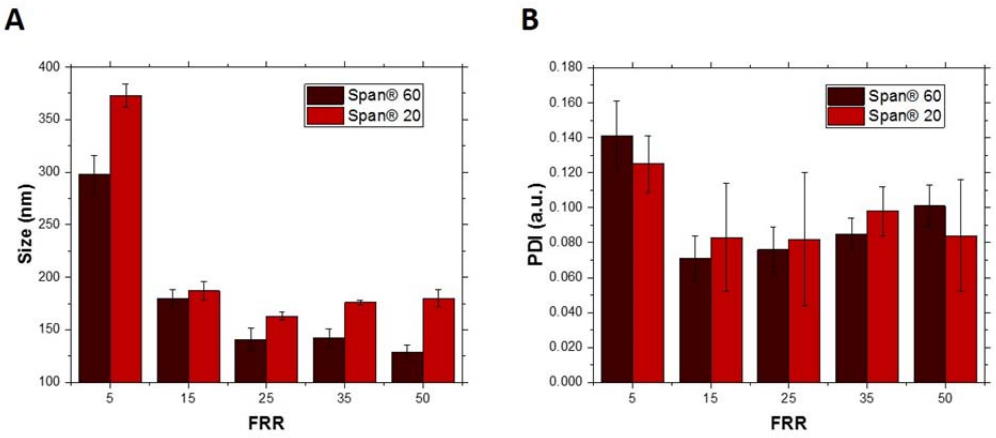
A
B
Size (nm)
PDI (a.u.)
FRR
FRR
Span® 60
Span® 20
Span® 60
Span® 20
400
350
300
250
200
150
100
0.180
0.160
0.140
0.120
0.100
0.080
0.060
0.040
0.020
0.000
5
15
25
35
50
5
15
25
35
50

Figure 7.